Can the Uncertainties of Madden–Jullian Oscillation Cause a Significant "Spring Predictability Barrier" for ENSO Events?

PENG Yuehua[1,2,3] (彭跃华), DUAN Wansuo[2*] (段晚锁), and XIANG Jie[3] (项 杰)

1 *Dalian Naval Academy, Dalian* 116018

2 *LASG, Institute of Atmospheric Physics, Chinese Academy of Sciences, Beijing* 100029

3 *Institute of Meteorology, PLA University of Science and Technology, Nanjing* 211101

(Received October 14, 2011; in final form August 2, 2012)

ABSTRACT

With the Zebiak-Cane model and a parameterized stochastic representation of intraseasonal forcing, the impact of the uncertainties of Madden–Jullian Oscillation (MJO) on the "Spring Predictability Barrier (SPB)" for El Niño–Southern Oscillation (ENSO) prediction is studied. The parameterized form of MJO forcing is added physically to the Zebiak-Cane model to obtain the so-called Zebiak-Cane-MJO model and then the effects of initial error, stochastic model error, and their joint error mode on the SPB associated with El Niño prediction are estimated. The results show that the model errors caused by stochastic MJO forcing could hardly lead to a significant SPB while initial errors can do; furthermore, the joint error mode of initial error and model error associated with the stochastic MJO forcing can also lead to a significant SPB. These demonstrate that the initial error is probably the main error source of the SPB, which may provide a theoretical foundation of data assimilation for ENSO forecasts.

Key words: ENSO, MJO, SPB, Zebiak-Cane model

Citation: Peng Yuehua, Duan Wansuo, and Xiang Jie, 2012: Can the uncertainties of Madden–Jullian Oscillation cause a significant "spring predictability barrier" for ENSO events? *Acta Meteor. Sinica*, **26**(5), 566–578, doi: 10.1007/s13351-012-0503-7.

1. Introduction

El Niño–Southern Oscillation (ENSO) is the most prominent interannual signal in the climate system and has large effects on global climate. Knowledge about the ENSO cycle and the ability to forecast its variations supply valuable information for agriculture, public health and safety, fisheries, forestry, and many other spheres of climate-sensitive human endeavor (Huang, 1999; Zhang et al., 2003). It is therefore very important to simulate and predict ENSO.

While significant progress has been made in ENSO theories and predictions over the years, there still exist considerable uncertainties in realistic ENSO predictions (Tang et al., 2008; Luo et al., 2008). In particular, for forecasts made before and throughout the late spring–early summer, ENSO predictions tend to be much less successful. This low predictability has been related to the so-called "spring predictability barrier (SPB)" of ENSO (Webster and Yang, 1992). The SPB is a well-known characteristic of ENSO forecasts (Webster and Yang, 1992; Lau and Yang, 1996; Moore and Kleeman, 1996; Chen et al., 2004), which refers to the phenomenon that most ENSO prediction models often experience an apparent drop in prediction skill across May and June (Latif et al., 1994). Considerable efforts have been made in studying this phenomenon, but its physical reason remains controversial. One possible cause is the rapid seasonal transition of monsoon circulation during the boreal spring, which perturbs the Pacific Ocean's basic state when the east-west sea surface temperature (SST) gradient is at its weakest (Webster and Yang, 1992; Lau and Yang, 1996). Another notion, proposed by Webster (1995), is that SPB

Sponsored by the Knowledge Innovation Program of the Chinese Academy of Sciences (KZCX2-YW-QN203), National Basic Research and Development (973) Program of China (2010CB950400 and 2012CB955202), and National Natural Science Foundation of China (41176013).

*Corresponding author: duanws@lasg.iap.ac.cn.

is caused by the fact that the ocean-atmosphere coupling is the weakest during April and May in the eastern Pacific. Other studies have argued that SST anomalies (SSTA) in the boreal spring are relatively small, making them difficult to detect and forecast in the presence of atmospheric and oceanic noises (Chen et al., 1995). Recently, Mu et al. (2007a) demonstrated that the SPB may result from the combined effect of the climatological mean equilibrium state, the El Niño event itself, and initial error patterns.

Many studies have investigated the SPB of ENSO from the perspective of initial error growth. Moore and Kleeman (1996) utilized the approach of linear singular vector (LSV) and revealed the impact of initial perturbation on ENSO predictability. Xue et al. (1997) also used LSV and demonstrated that the ENSO prediction level was dependent on the precision of initial fields of a numerical model. Chen et al. (1995, 2004) reduced the SPB and enhanced ENSO prediction skill of the Zebiak-Cane model by improving the model initialization. Recently, Mu et al. (2007a, b) and Duan et al. (2009a) further studied the ENSO predictability and illustrated the effect of the transient growth of initial perturbations caused by nonlinear instability, concluding that the initial perturbations with specific spatial structure can lead to significant SPB. Duan et al. (2009b) and Yu et al. (2009) recognized two types of initial perturbations using statistical and dynamical methods, respectively, and demonstrated the dynamical mechanisms of error growth related to SPB.

The above studies have mainly investigated the effect of initial perturbations on the SPB of ENSO. In general, the uncertainty of climate prediction is caused by both initial perturbation and model perturbation (i.e., model error). The effect of model perturbation on ENSO predictability is also a meaningful subject worthy of investigation. Duan and Zhang (2010) compared the effects of initial perturbation and model perturbation caused by parameter uncertainties in the model on ENSO predictability with a theoretical ENSO model. Their results showed that, compared with the initial perturbation, the prediction error yielded by parameter uncertainties related to model error was relatively small and did not have a significant impact on ENSO predictability. The uncertainty of external forcing is also an important source of model perturbation. How does the uncertainty of external forcing affect the SPB of ENSO?

The intraseasonal oscillation or Madden–Jullian oscillation (ISO/MJO) is one of the main external forcing of ENSO, but the relationship between MJO and ENSO is still greatly disputable. One point of view insisted that MJO was one of the mechanisms provoking El Niño events and had a significant effect on ENSO events (Sperber et al., 1997; McPhaden, 1999; Zhang, 2001: Cravatte et al., 2003; Rong et al., 2011). For example, Rong et al. (2011) proposed that the winds of high frequency including MJO could rectify the surface wind stress of low frequency on the interannual timescale through nonlinearity, which could significantly modulate the ENSO variability. However, other studies argued that MJO had little influence on El Niño (Zebiak, 1989; Hendon et al., 1999; Slingo et al., 1999; Kessler and Kleeman, 2000). For example, Slingo et al. (1999) and Hendon et al. (1999) demonstrated that the correlativity between the interannual variation of MJO and the SSTA of El Niño was very weak. Therefore, it is necessary to further study the effect of MJO forcing on ENSO. Using the Zebiak-Cane model and a parameterized form of the MJO forcing, Peng et al. (2011) indicated that the uncertainties of MJO had little effect on the maximum prediction error for ENSO events caused by conditional nonlinear optimal perturbations. What about the effect on SPB?

In this paper, we will explore the effect of stochastic MJO forcing on the SPB of ENSO and attempt to compare the impacts of initial perturbation and stochastic model perturbation caused by MJO uncertainty on ENSO predictability quantitatively. The paper is organized as follows. In Section 2, the Zebiak-Cane model and the parameterized form of stochastic MJO forcing are described and the approach called Conditional Nonlinear Optimal Perturbation (CNOP) is also introduced. In Section 3, we report the main results of numerical experiments and show the effect of MJO uncertainty on the SPB of ENSO. Finally, conclusions and discussion are presented in Section 4.

2. Model and methodology

2.1 Zebiak-Cane model

The Zebiak-Cane model (Zebiak and Cane, 1987) was the first coupled ocean-atmosphere model to simulate the interannual variability of the observed ENSO and has been a benchmark in the ENSO community for over two decades. The Zebiak-Cane model has been widely used in predictability studies and predictions of ENSO (Zebiak and Cane, 1987; Blumenthal, 1991; Chen et al., 2004; Tang et al., 2008). It is composed of a Gill-type steady state linear atmospheric model and a reduced-gravity oceanic model. The Zebiak-Cane model depicts the thermodynamics and atmospheric dynamics in the tropical Pacific with oceanic and atmospheric anomalies about the mean climatological state specified from observations (see Zebiak and Cane, 1987).

In the model run, the atmospheric model is previously run with the specified monthly mean SST anomalies to simulate monthly mean wind anomalies. Then, the oceanic model is forced by surface wind stress anomalies that are generated from a combination of the surface wind anomalies produced by the atmosphere model and the background mean winds.

2.2 MJO forcing

In this paper, the effect of stochastic MJO forcing on ENSO predictability is studied but this type of forcing is not considered in the Zebiak-Cane model. Therefore, it is necessary to introduce a rational fashion of MJO forcing into the Zebiak-Cane model. Zebiak (1989) constructed a parameterized form of MJO forcing according to the observation and investigated the effect of MJO on ENSO prediction.

The rules of MJO are usually as follows: (1) the low-level wind signal is dominantly zonal in the equatorial region; (2) the 30–60-day period band contains most of the power; and (3) the disturbances are energetic in western Pacific, but weaker (at the surface) in eastern Pacific. Therefore, the MJO fashion determined by Zebiak (1989) is as follows:

$$\tau^{(x)}(t) = A[R(t) + 2R(t-\Delta t) + R(t-2\Delta t)] \cdot\cos(\omega_0 t + t_0)\frac{\exp\Big[-\Big(\frac{y}{10}\Big)^2\Big]}{\exp\Big[-\Big(\frac{x-x_0}{10}\Big)^2\Big]}, \quad (1)$$

where R is a normal random variable with zero mean and unit variance, and t_0 represents a uniform random variable on $(0, 2\pi)$. This forcing is evaluated at time intervals of Δt, which for the Zebiak-Cane model is 10 days. The parameters ω_0 and x_0 were taken to be $2\pi/40$ days and 146°E, respectively, and the amplitude A was set at 0.015 N m^{-2}. The western Pacific region (5°N–5°S, 163.125°E–163.125°W) was forced by the MJO forcing.

Figure 1 shows the three 48-month realizations of this forcing function. Anomalies as large as the climatological mean stress (about 0.05 N m^{-2}) occur frequently; the model forcing is as strong as or probably stronger than what is observed (Madden, 1988; see his Fig. 3). Therefore, the parameterized form of MJO is feasible.

The parameterized stochastic MJO forcing has a large uncertainty. What is the evolution of the uncertainty? Compared with initial perturbation, how will it affect the SPB of ENSO?

2.3 Conditional Nonlinear Optimal Perturbation

The CNOP is an initial perturbation that satisfies a given constraint and has the largest nonlinear evolution at the prediction time. The CNOP approach is a natural generalization of the Linear Singular Vector (LSV) approach to the nonlinear regime. It has been used to study the nonlinear dynamics of ENSO

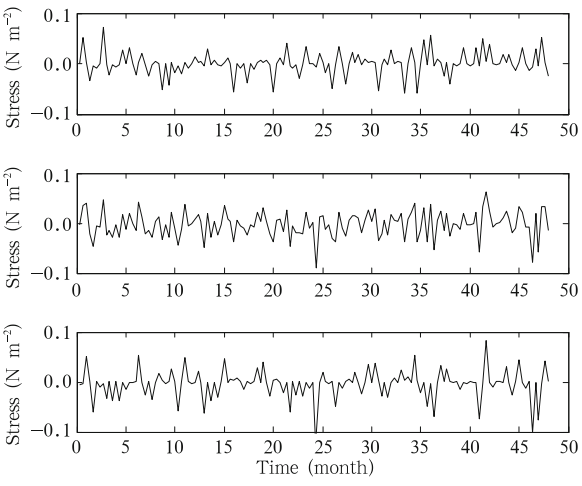

Fig. 1. Three 48-month realizations of the stochastic MJO wind stress forcing (N m^{-2}).

predictability (Mu and Duan, 2003; Duan et al., 2004; Duan and Mu, 2006; Mu et al., 2007a, b; Peng et al., 2011) and the sensitivity of ocean circulation (Mu et al., 2004). Recently, the CNOP approach has also been used to generate initial perturbations for ensemble prediction (Mu and Jiang, 2008) and determine the "sensitive area" in target observations for typhoons (Mu et al., 2009). These studies have shown that CNOP is a useful tool for studying weather and climate predictability.

In order to compare the initial perturbation with model perturbation caused by stochastic MJO forcing on ENSO predictability, we calculate the initial perturbation which has the largest impact on El Niño forecast at prediction time and can amount to a maximum prediction error with the CNOP approach (i.e., CNOP error). The CNOP error in this paper is calculated as follows:

We construct a cost function to measure the evolution of initial perturbation. The aforementioned CNOP, denoted by $u_{0\delta}$, can be obtained by solving the following nonlinear optimization problem

$$J(\boldsymbol{u}_{0\delta}) = \max_{\|\boldsymbol{u}_0\| \leqslant \delta} \|\boldsymbol{T}'(\tau)\|_2, \tag{2}$$

where $\boldsymbol{u}_0 = (w_1\boldsymbol{T}'_0, w_2\boldsymbol{h}'_0)$ is a non-dimensional initial perturbation of the SSTA and thermocline depth anomaly superimposed on the initial state of a predetermined reference-state El Niño event. Items $w_1 = (2℃)^{-1}$ and $w_2 = (50\ \mathrm{m})^{-1}$ are the characteristic scales of SST and thermocline depth, which are used to make the initial errors T_0 and h_0 nondimensional. These characteristic scales are derived by scale analysis and they agree reasonably wel1 with observations (Wang and Fang, 1996). The constraint condition $\|\boldsymbol{u}_0\| \leqslant \delta$ is defined by a prescribed positive real number δ and the norm $\|\boldsymbol{u}_0\| = \sqrt{\sum_{i,j}[(w_1\boldsymbol{T}'_{0i,j})^2 + (w_2\boldsymbol{h}'_{0i,j})^2]}$, where $\boldsymbol{T}'_{0i,j}$ and $\boldsymbol{h}'_{0i,j}$ represent the dimensional initial perturbation of the SSTA and thermocline depth anomaly at different grid points and (i, j) is the grid point in the domain of the tropical Pacific with latitude and longitude from 19°S to 19°N by 2° and from 129.375°E to 84.375°W by 5.625°, respectively. The evolution of the initial perturbation is measured by $\|\boldsymbol{T}'(\tau)\|_2 = \sqrt{\sum_{i,j}(T'_{i,j}(\tau))^2}$, where $\boldsymbol{T}'(\tau)$ represents the prediction error of SSTA at time τ and is obtained by subtracting the SSTA of the reference state from the predicted SSTA at prediction time τ.

3. Effects of MJO uncertainty on the SPB of ENSO predictions

From the perspective of error growth, the SPB phenomena in ENSO predictions mean two points. One is that the error growth is maximum in some special season and the other is that the error growth has significant effect on the prediction results.

As stated above, MJO is one of the main external forcing for ENSO events. However, the simulation of MJO has great uncertainty internationally. Many researchers use parameterized form of MJO such as the stochastic form introduced in Section 2. The stochastic MJO forcing is unpredictable because of its randomness so it can be regarded as a stochastic model perturbation. How do the stochastic model perturbations evolve and what is their impact on the SPB of ENSO? Compared with initial perturbation, which one has a larger impact? In this section, we will adopt the stochastic MJO fashion to address these questions.

3.1 Experimental design

Integrating the Zebiak-Cane model for 1000 yr, we obtain a time series of SSTA, which provides a great number of El Niño events. These El Niño events tend to have a 4-yr period and phase-lock to the end of the calendar year. In numerical experiments, we choose many El Niño events and find that the results depend on the intensities of El Niño events. Therefore, two groups of El Niño events are used to describe the results: one group consists of weak events with Niño-3 index (the SSTA averaged over the Niño-3 region (5°S–5°N, 90°–150°W)) less than 2.5℃; the other group include strong events, with Niño-3 index larger than 2.5℃. Considering that there are different types of El Niño events in nature, we choose four events in each group with initial warming occurring in January, April, July, and October.

For convenience, we call the Zebiak-Cane model with MJO forcing the Zebiak-Cane-MJO model. We

are able to investigate the model perturbations caused by stochastic MJO forcing on ENSO predictability with this Zebiak-Cane-MJO model to forecast the above El Niño events. In fact, integrating the Zebiak-Cane-MJO model with original states of El Niño events as initial value can lead to the El Niño events under the influence of model perturbations yielded by stochastic MJO forcing. Comparing the uncertain El Niño events with reference state events, their difference is the prediction error caused by stochastic MJO forcing for El Niño events.

For each prediction, we calculate the CNOP-type initial perturbations with optimization time length of 12 months. In order to investigate the impact of CNOP-type initial perturbations on the SPB of ENSO events, we explore the seasonal evolutions of prediction errors. One year is divided into four seasons: starting with January to March (JFM), followed by April to June (AMJ), and so forth. The AMJ season is the time when the SPB occurs in most ENSO prediction models (Latif et al., 1994; Webster and Yang, 1992). Many studies used the error growth rate during this season to measure the SPB (Moore and Kleeman, 1996; Mu et al., 2007a, b). In this paper, we also use the error growth rate during the AMJ season to study the SPB. We calculate the slope of the curve defined by $\gamma(t) = \|T'(t)\|_2$ in each season, where $T'(t)$ denotes the SSTA component in the nonlinear evolution of CNOP-type initial perturbations. The slope marked by κ shows the growth rate of CNOP-type initial perturbations in each season. A positive value of κ denotes increscent error growth and larger absolute values mean faster error growth. Furthermore, by adding the CNOP errors in the start month of El Niño prediction and integrating Zebiak-Cane model with the perturbed initial values, we obtain the prediction errors caused by CNOP-type initial perturbations for ENSO events. The prediction error is denoted by the Niño-3 index in the nonlinear evolution of CNOP in the prediction time and marked by $E_{\text{Niño-3}}$ (Xu, 2006). The negative (positive) values of $E_{\text{Niño-3}}$ indicate an under-prediction (over-prediction) of the event and larger absolute values mean less predictability. In this paper, the condition of prediction obstacle is $|E_{\text{Niño-3}}| > 0.5$℃.

In the context, we use Year (0) to denote the year when El Niño attains a peak value, and Year (–1) and Year (1) to signify the year before and after Year (0), respectively. For each El Niño event, we make predictions for 12 months with different start-months. In numerical experiments, the El Niño predictions are made with start-months of Jul(–1) (i.e., July in Year (–1)), Oct(–1), Jan(0), Apr(0), Jul(0), Oct(0), Jan(1), or Apr(1).

3.2 Results

For convenience, the strong and weak events with initial warming in January, April, July, and October, are denoted by SR_i (SR) and WR_i (WR) ($i = 1, 2, 3, 4$). Figure 2 shows the time-dependent Niño-3 indices for these 8 El Niño events. It is obvious that the El Niño events with initial warming in January and April such as SR_1, SR_2, WR_1, and WR_2 usually reach peak values in the first year and those with initial warming in July and October such as SR_3, SR_4, WR_3, and WR_4 reach the peak values in the second year. The solid spots and triangles indicate the start-months of the growth-phase predictions and decaying-phase predictions, respectively. The period between Apr(0) and Jul(0) is the spring of growth-phase and that between Apr(1) and Jul(1) is the spring of decaying-phase.

3.2.1 Characteristics of the seasonal evolutions of the prediction errors caused by CNOP-type initial perturbations

Yu et al. (2009) investigated the SPB problem for El Niño events by tracing the evolution of CNOP. Their results showed that the evolution of CNOP-type errors had obvious seasonal dependence and yielded a significant SPB. In addition, the growth-phase prediction uncertainties caused by the CNOP-type errors were larger than the corresponding uncertainties for the decaying-phase prediction. Meanwhile, El Niño predictions with a start-month in spring (i.e., from Apr(0)) were relatively easier than those with a start-month in other seasons (see details in their Fig. 5). Our results are similar to them. For conciseness, we only take an example. The seasonal growth rates and Niño-3 prediction errors with start-month of Oct(–1) for 8 El Niño events are given in Table 1. The maxi-

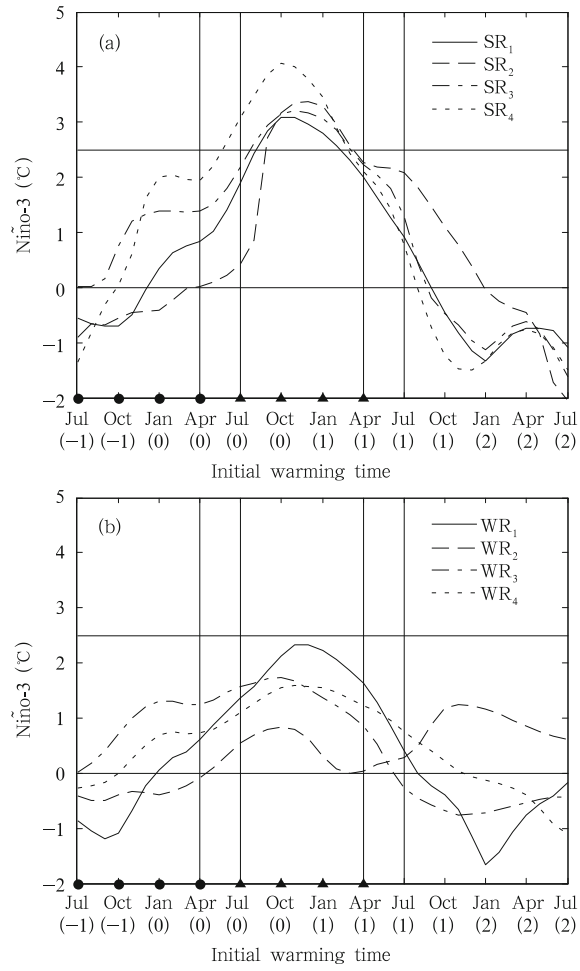

Fig. 2. Two groups of reference-state El Niño events with initial warming time in Jul(–1), Oct(–1), Jan(0), Apr(0), respectively. (a) The time-dependent Niño-3 indices of 4 strong El Niño events denoted by SR_i, $i = 1$, 2, 3, and 4; and (b) those of 4 weak El Niño events denoted by WR_i, $i = 1$, 2, 3, and 4.

mum values of error growth rates for each event are highlighted by overstriking and underlining and the values of Niño-3 prediction errors are distinguished in italics. It can be seen that the maximum error growth rates are all greater than 7 and the prediction errors of Niño-3 index are entirely larger than 1℃, which exceed the condition of prediction barrier; besides, the maximum error growth rates for the reference events are almost in the AMJ season except the weak events with initial warming in October. Apparently, the CNOP-type initial perturbations can lead to severe spring predictability barrier for El Niño events predicted from Oct(–1).

Table 1. The growth rates of initial perturbations for 8 events predicted from Oct(–1)

Init	OND	JFM	AMJ	JAS	$E_{\text{Niño3}}$
WR_1	1.7501	3.9987	**8.0451**	–2.8675	*–1.1490*
WR_2	3.0809	3.7609	**7.7913**	5.2991	*1.8479*
WR_3	1.2283	2.4731	**7.7042**	5.2004	*1.5436*
WR_4	1.4885	2.4774	7.8240	**9.0196**	*1.9719*
SR_1	4.1135	1.7457	**9.3603**	3.9173	*–1.4659*
SR_2	2.7800	3.2787	**9.4053**	–0.3463	*–1.2352*
SR_3	1.5973	2.4342	**9.2742**	5.8997	*–1.6095*
SR_4	2.3112	4.3354	**7.9843**	2.2110	*–1.1347*

3.2.2 Seasonal evolution characteristics of model perturbations caused by stochastic MJO forcing

The MJO form depicted by Eq. (1) in Section 2 includes stochastic item. Owing to the randomness, every numerical realization of the stochastic item will have different results; thus, diverse realizations of the MJO form of Eq. (1) will have diverse results. Similar to Zebiak (1989), for each El Niño event, the stochastic wind stresses of MJO forcing are numerically realized for 9 times to get 9 different kinds of MJO forcing. In the numerical experiments, we insert each one of 9 MJO realizations as external forcing into the Zebiak-Cane model, and then explore the seasonal evolution characters of model perturbation caused by stochastic MJO forcing for El Niño events. The results show that, for the 8 types of MJO forcing and 9 El Niño events, the seasonal growth rates of stochastic model perturbations predicted from Jul(–1), Oct(–1), Jan(0), Apr(0), Jul(0), Oct(0), Jan(1), and Apr(1) lasting for 12 months are all on the small side and their prediction errors of Niño-3 indices are almost less than 0.5℃. The values of maximum error growth rate are nearly less than 5 and the season-dependence is not obvious. Therefore, the model perturbations caused by stochastic MJO forcing basically cannot lead to significant SPB. To illuminate the results more clearly, Table 2 lists the error growth rates and prediction errors for 8 events predicted from Oct(–1) for 12 months. All of the predictions use the same numerical MJO forcing. It is obvious that the absolute values of error growth rate are almost less than 5 and the prediction errors are less than 0.5℃ except for one event; thus, it can be inferred that there is no predictability barrier. Moreover, the maximum error growth rates come forth

three times in OND season and twice in JFM and JAS season, respectively, so the season-dependence of error growth rates is not distinct. Hence, from the perspective of error growth, the model perturbations caused by stochastic MJO forcing could not lead to the SPB predicted from Jan(0) for El Niño events.

The results of Duan and Zhang (2010) indicate that the parameter errors in model could not result in significant SPB, uniting the results in this section. Therefore, we can deduce that initial perturbations are probably the main error source of SPB.

Table 2. The growth rates of stochastic model perturbations for 8 events predicted from Oct(–1)

Model	OND	JFM	AMJ	JAS	$E_{\text{Niño3}}$
WR_1	0.6078	0.4776	1.0317	**2.0969**	*0.0253*
WR_2	–0.2865	**1.5528**	0.1118	1.1017	*–0.2662*
WR_3	0.5375	–0.6277	**0.8042**	0.0301	*0.1227*
WR_4	1.2959	0.6671	0.4200	**5.4320**	*0.5495*
SR_1	**1.4420**	0.1091	0.1488	0.7779	*0.0027*
SR_2	–0.4418	**2.1399**	0.0343	–0.0307	*0.1683*
SR_3	**1.7079**	0.1386	1.4967	0.2011	*0.2673*
SR_4	**1.9025**	0.1285	–0.4826	1.8193	*0.0724*

3.2.3 Characteristics of the seasonal evolutions of the prediction errors caused by joint mode of initial perturbations and MJO uncertainties

In the actual ENSO forecast, the initial perturbation and stochastic model perturbation exist at the same time. Therefore, we further investigate the seasonal evolution characteristics of the prediction errors caused by joint mode of initial perturbation and model perturbation caused by stochastic MJO forcing. Considering the effect of CNOP errors in the initial field of the Zebiak-Cane-MJO model and integrating the model, we can produce the El Niño events under the influence of the joint mode of CNOP-type initial perturbations and model perturbations yielded by stochastic MJO forcing. The differences between these events and those generated by integrating the Zebiak-Cane model represent the evolutions of joint perturbation mode. After exploring the seasonal error growth rates and the prediction errors of Niño-3 indices, we find that in terms of error growth, the joint perturbation mode can lead to a significant SPB and the season-dependence is comparatively obvious but weaker than that of initial perturbation. In order to compare with the aforementioned results of initial perturbation and stochastic model perturbation, Tables 3–4 show the results of seasonal error growth rates and prediction errors predicted from Oct(–1) and Jan(0) for 12 months, respectively. All of the predictions correspond to the same numerical MJO forcing.

It can be seen from Table 3 that the values of maximum error growth rates in all events are larger than 5, some even reach 11, and the absolute values of prediction errors are entirely larger than 1℃, some even attain 2, so the predictability barrier is clear. Furthermore, the maximum error growth rates mostly appear in AMJ season except for the strong event with initial warming in July and the weak event with initial warming in October. Hence the joint perturbation mode can lead to a significant SPB for the El Niño events predicted from Oct(–1). The season-dependence is weaker than that of initial perturbations, which is possibly due to the disturbance of stochastic model perturbation, but the results are considerably similar to those of initial perturbation in general.

From Table 4, it is obvious that the error growth rates are comparatively large and the prediction errors are completely larger than 0.5℃, so the predictability barrier could happen. Besides, the maximum error growth rates almost appear in JAS season and the error growth rates in AMJ season have one maximum value and 5 secondary values. For this situation, Mu et al. (2007b) argued that although the largest growth of initial errors occurs in JAS season, the error growth during AMJ has become aggressively large and may have caused the drastic decrease in El Niño forecast skill across the spring. Therefore, we consider that the joint perturbation mode could lead to SPB for El Niño events predicted from Jan(0). In fact, the results of initial perturbations predicted from Jan(0) are

Table 3. The seasonal growth rates of joint perturbation mode for 8 events predicted from Oct(–1)

Join	OND	JFM	AMJ	JAS	$E_{\text{Niño3}}$
WR_1	2.1887	5.0858	**6.8802**	–4.8951	*–1.2181*
WR_2	2.5017	1.9534	**8.3581**	4.1918	*1.6379*
WR_3	0.1449	2.7917	**9.5892**	5.4973	*1.7325*
WR_4	0.9888	4.4941	8.1599	**11.7583**	*2.3843*
SR_1	3.4477	1.9840	**8.9405**	4.8789	*–1.4350*
SR_2	1.3172	2.4356	**5.6193**	2.2599	*–1.0179*
SR_3	2.8446	2.8533	4.7334	**6.9878**	*–1.4613*
SR_4	3.4896	5.3163	**11.3255**	6.3741	*–2.1082*

Table 4. The seasonal growth rates of joint perturbation mode for 8 events predicted from Jan(0)

Join	JFM	AMJ	JAS	OND	$E_{\text{Niño3}}$
WR_1	2.2993	**9.2758**	**10.6225**	–4.9738	*2.0861*
WR_2	1.1245	**6.6403**	**10.1522**	–4.0097	*1.6258*
WR_3	2.0115	**3.4337**	**4.9375**	–0.0768	*–0.8079*
WR_4	1.6789	2.3396	**4.5639**	**3.4543**	*1.1686*
SR_1	1.7925	**6.7274**	**9.3316**	–2.5935	*–1.1370*
SR_2	1.7476	0.9020	**3.0141**	**1.8248**	*–0.6540*
SR_3	1.4106	**6.8548**	**4.2088**	–1.0742	*–1.0742*
SR_4	3.8473	**8.2800**	**8.9280**	–3.8812	*–1.6346*

Note: bold numbers without underlines indicate the second largest values.

mostly the same.

The results also indicate that the model perturbations caused by stochastic MJO forcing contribute little to SPB; thus, initial perturbations are likely the main error source of SPB in ENSO prediction.

3.2.4 Comparison of seasonal evolutions of prediction errors caused by initial perturbation, stochastic model perturbation, and joint perturbation mode

In order to visually show more results, we contrast the characteristics of seasonal evolutions of prediction errors caused by initial perturbation, stochastic model perturbation, and joint perturbation mode, and compare them in the same histogram. The error growth rates of 8 events are analogous, so we use their ensemble mean to plot histograms. As for the prediction errors of Niño-3 indices, we analyze them with other histograms. The seasonal growth rates of stochastic model perturbation, initial perturbation, and joint perturbation mode with 4 types of numerical MJO forcing predicted from Jul(–1) are shown in

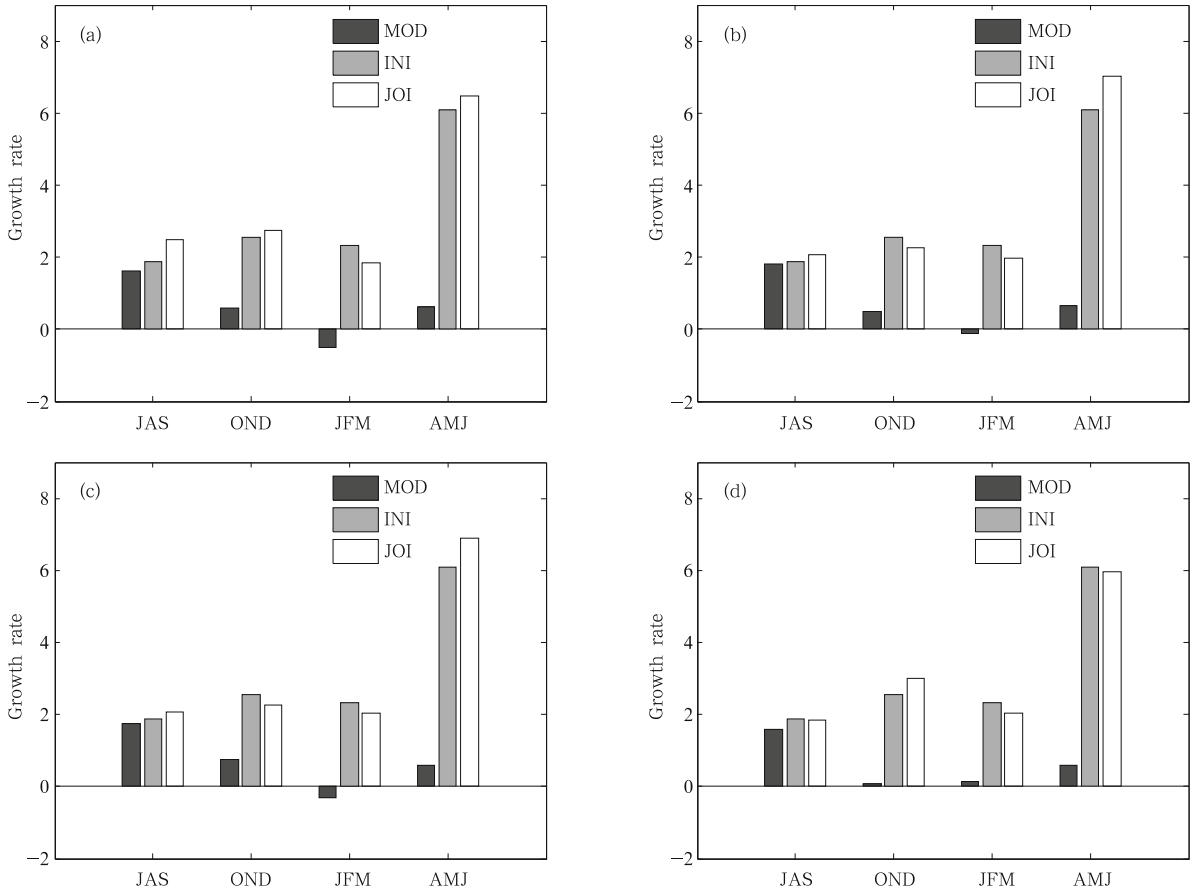

Fig. 3. The seasonal growth rates of stochastic model perturbation, initial perturbation, and joint perturbation mode, with 4 (a, b, c, and d) of 9 types of numerical MJO forcing predicted from Jul(–1). The symbol "MOD" stands for the prediction errors yielded by the stochastic MJO forcing; "INI" indicates those caused by initial perturbation; "JOI" indicates those resulting from the joint mode of both initial perturbation and stochastic model perturbation.

Fig. 3. It illustrates that, for all of the forcing, there are two common conclusions. On the one hand, the values of seasonal growth rates of initial perturbation and joint perturbation mode are pretty near, while those of stochastic model perturbation are comparatively far less. On the other hand, the season-dependence of joint error growth rate is the same as initial error growth rate and their maximum values appear in AMJ season (i.e., spring), while the maximum growth rates of stochastic model perturbation appear in JAS season. For different forcing, in the same season, the error growth rates of initial perturbation are uniform and joint ones are pretty much the same, while model ones are discrepant; some even have opposite signs such as the error growth rates of JFM are plus in Fig. 3d but they are minus in Figs. 3a, 3b, and 3c.

On the whole, seasonal error growth rates of different MJO forcing are similar (i.e., the 4 pictures in Fig. 3 are similar), so we just contrast the results under the same MJO forcing but predicted from different months. Figure 4 shows the seasonal growth rates of stochastic model perturbation, initial perturbation, and joint perturbation mode with the same numerical MJO forcing predicted from Jul(–1), Oct(–1), Jan(0), and Apr(0). The common results of 4 pictures are as follows: the error growth rates of initial perturbation are close to those of joint ones while the model ones are far less; moreover, the seasons during which the maximum seasonal growth rates of joint perturbation mode appear are the same as those of initial perturbation, but those of stochastic model perturbation are usually different with them. These results illustrate that stochastic model perturbation could hardly yield a significant SPB and their contribution to SPB caused by joint perturbation mode is little. In fact, it further

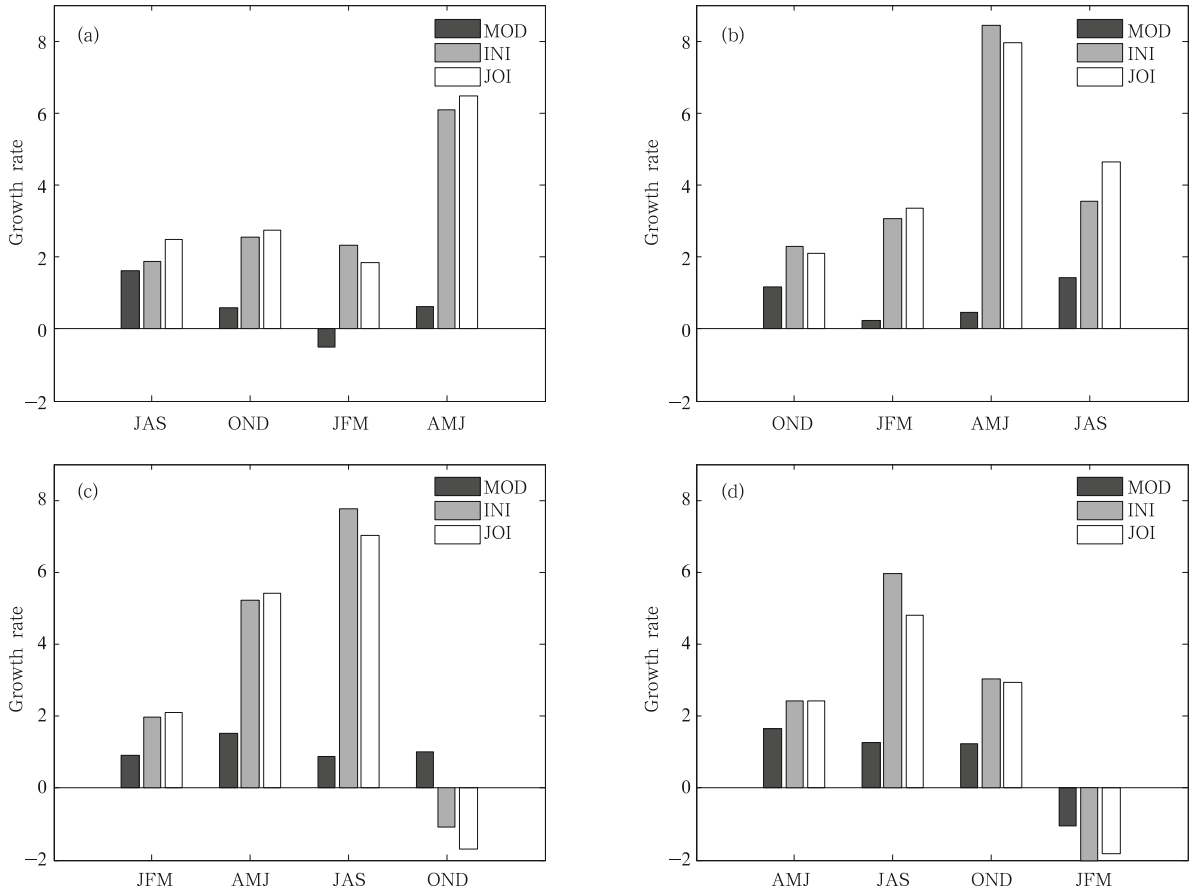

Fig. 4. The seasonal growth rates of stochastic model perturbation, initial perturbation, and joint perturbation mode with the same numerical MJO forcing predicted from (a) Jul(–1), (b) Oct(–1), (c) Jan(0), and (d) Apr(0).

emphasizes that initial perturbation is the main error source leading to SPB. For different initial predicting months, the maximum growth rates of initial perturbation and joint perturbation mode predicted from Jul(–1) and Oct(–1) are fully in AMJ season, while those predicted from Jan(0) and Apr(0) are in JAS season but those of stochastic model perturbation are season inconstant. The results about initial perturbation are consistent with former studies (e.g., Yu et al., 2009).

As regards the prediction errors of Niño-3 index, we do not use ensemble mean because the result of every event has specific meaning. The prediction errors for 8 events predicted from Jul(–1), Oct(–1), Jan(0), and Apr(0) are displayed in Fig. 5, in which all predictions correspond to the same numerical MJO forcing. It can be seen that the CNOP-type initial perturbation leads to large prediction errors for El Niño events but the prediction errors caused by stochastic MJO forcing are far less than those by initial perturbation. On the condition that $|E_{\text{Niño-3}}| > 0.5$℃ would cause predictability barrier, initial perturbation could yield severe predictability barrier while stochastic model perturbation basically could not lead to such a result. Besides, the prediction errors caused by joint perturbation mode and initial perturbation have less distinction. This indicates that model perturbations caused by stochastic MJO forcing contribute little to SPB;

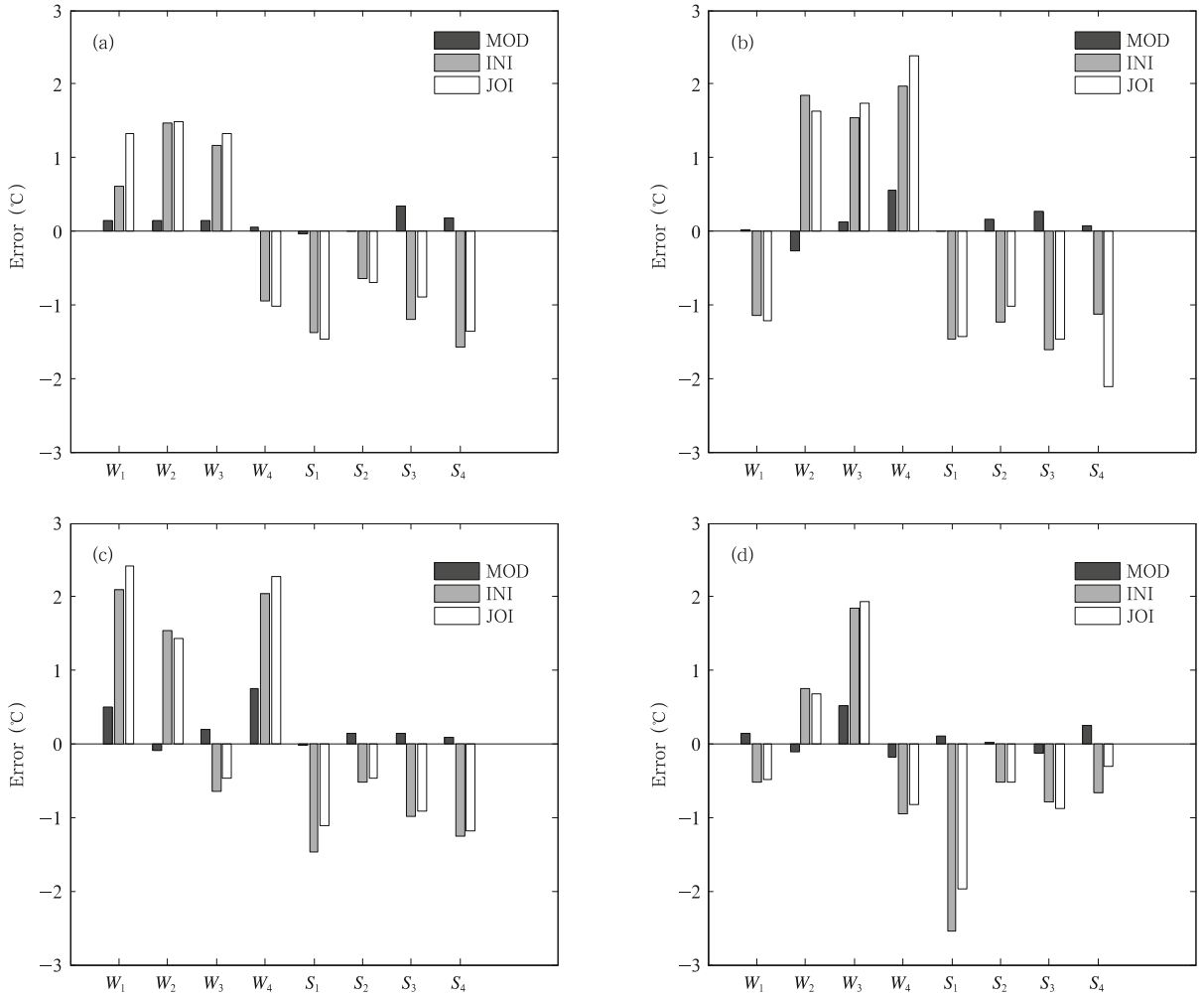

Fig. 5. Prediction errors of Niño-3 indices of the 8 El Niño events with start-moths of (a) Jul(–1), (b) Oct(–1), (c) Jan(0), and (d) Apr(0). All the predictions correspond to the same numerical MJO forcing. W_i denotes weak El Niño events and S_i denotes strong El Niño events.

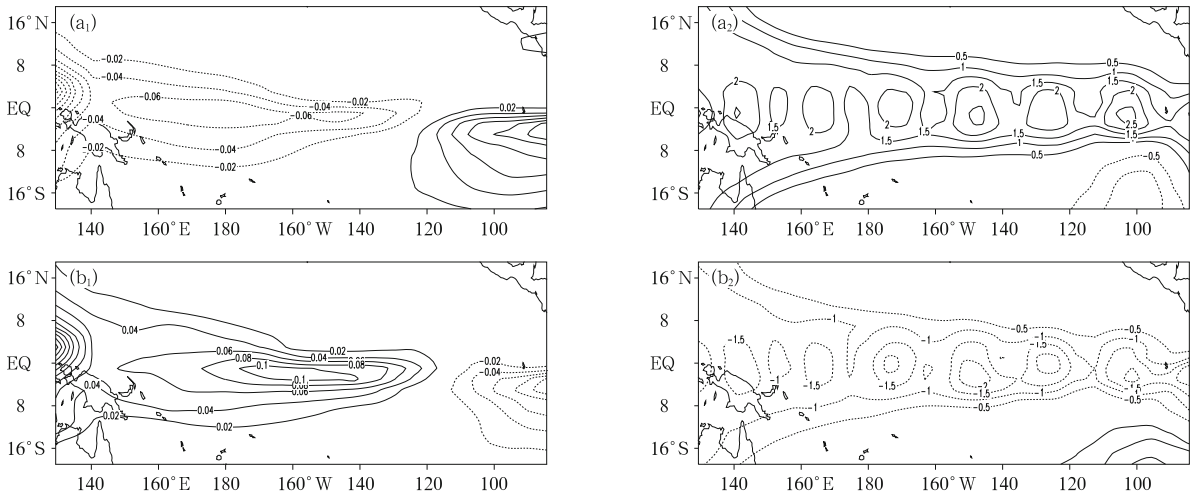

Fig. 6. Distribution patterns of two categories of CNOP errors. Left column is for the SSTA component, and right column is for the thermocline depth anomaly. (a) Type-1 CNOP errors and (b) type-2 CNOP errors.

hence, initial perturbations are the main error source of SPB.

What is more, since the negative (positive) values of $E_{\text{Niño-3}}$ indicate an under-prediction (over-prediction) of the event, from Fig. 5, we can see that CNOP errors and joint perturbation mode almost under-predict the El Niño events for strong events while they mostly over-predict the events for weak El Niño events. The reason is that the CNOP-type errors related to these predictions can be classified into two types. We refer to these two kinds of CNOP-type errors as type-1 and type-2 CNOP errors, respectively. The CNOP errors superimposed on the strong El Niño events consist of the type-1 errors that possess an SSTA pattern with negative anomalies in the equatorial central-western Pacific, positive anomalies in the equatorial eastern Pacific, and a thermocline depth anomaly (TDA) pattern with deepening tendency along the equator (Fig. 6), which favors anomalous westerly and warm upwelled subsurface water and finally causes over-prediction of the corresponding event. The type-2 errors superimposed on the weak El Niño events are of SSTA and TDA patterns almost opposite to the former error patterns (Fig. 6), and they easily cause anomalous easterly and cool upwelled subsurface water, which tend to cause under-prediction of the event.

We also conducted an experiment to examine the effect of different MJO intensities on SPB. In the experiment, when the intensity is increased to triple of the original, the model error could yield SPB. However, considering that the intensity of the MJO in this paper is much accordant with the observation, we did not emphasize the SPB caused by the unreasonably strong MJO.

4. Summary and discussion

In this paper, a parameterized form of MJO forcing is introduced into the Zebiak-Cane model to obtain the so-called Zebiak-Cane-MJO model and the evolutions of initial perturbation, stochastic model perturbation, and their joint perturbation mode based on ENSO events are calculated. By investigating their error growth rates and prediction errors of Niño-3 indices, the main conclusions are as follows:

(1) The growth rates of joint perturbation mode and initial perturbation are close but those of stochastic model perturbation are clearly different with them. The growth rates of model perturbation are not significantly season-dependent while those of joint perturbation mode are pretty well season-dependent and most of them are the same as those of initial ones. Based on ensemble mean of eight events, only the growth rates

of model perturbation predicted from the same month with different MJO forcing have obvious distinction but those of joint ones are close.

(2) The CNOP-type initial perturbations could lead to large prediction errors for El Niño events and the results of joint perturbation mode are pretty much near, whereas prediction errors caused by stochastic MJO forcing are far less than those by initial perturbation. In terms of the prediction errors caused by initial perturbation and joint perturbation mode, strong events are underestimated while weak events are overestimated.

(3) Model perturbations caused by stochastic MJO forcing could not lead to a significant SPB and their contribution to SPB is small, so initial perturbations are probably the main error source causing SPB.

The results suggest that the precision of initial field should be paid more attention in ENSO prediction. We notice that the area of CNOP-type initial perturbation is concentrated and has obvious characteristic of locality. In fact, this CNOP error indicates the sensitive area of ENSO prediction. If we increase the observation in the sensitive area and reduce the opportunity of CNOP error in actual ENSO forecast, the forecast skill would possibly improve enormously. Moreover, the dependency of ENSO predictability on initial perturbation emphasized in this paper provides a theoretical base for the adaptive data assimilation of ENSO forecasts.

The work in this paper is not all-around and some results need further discussion and investigation. For example, if we use the actual observational MJO, do the results also support those with the parameterized MJO form in the paper? Besides, the Zebiak-Cane model used in the paper to study the effect of MJO on SPB in ENSO prediction is relatively simple and more complicated air-sea coupled model is needed to tackle the problem. Moreover, it is necessary to investigate whether the results are model-dependent. To sum up, the results of this study may be applied to improving the model and enhancing the ENSO forecast skill, while further research of the problems revealed in this paper is indispensable.

Acknowledgments. We thank the two anonymous reviewers for their helpful comments and suggestions.

REFERENCES

Blumenthal, M. B., 1991: Predictability of a coupled atmosphere-ocean model. *J. Climate*, **4**, 766–784.

Chen, D., S. E. Zebiak, and A. J. Busalacchi, 1995: An improved procedure for El Niño forecasting: Implications for predictability. *Science*, **269**, 1699–1702.

——, M. A. Cane, and A. Kaplan, 2004: Predictability of El Niño over the past 148 years. *Nature*, **428**, 733–736.

Cravatte, S., J. Picaut, and G. Eldin, 2003: Second and first baroclinic Kelvin modes in the equatorial Pacific at intraseasonal time-scales. *J. Geophys. Res.*, **108**(C8), 3266, doi: 10.1029/2002JC001511.

Duan, W. S., M. Mu, and B. Wang, 2004: Conditional nonlinear optimal perturbation as the optimal precursors for ENSO events. *J. Geophys. Res.*, **109**, D23105.

——, and ——, 2006: Investigating decadal variability of El Niño–Southern Oscillation asymmetry by conditional nonlinear optimal perturbation. *J. Geophys. Res.*, **111**, C07015, doi: 10.1029/2005JC003458.

——, F. Xue, and M. Mu, 2009a: Investigating a nonlinear characteristic of El Niño events by conditional nonlinear optimal perturbation. *Atmos. Res.*, **94**(1), 10–18.

——, X. C. Liu, K. Y. Zhu, and M. Mu, 2009b: Exploring the initial perturbations that cause a significant "spring predictability barrier" for El Niño events. *J. Geophys. Res.*, **114**, C04022, doi: 10.1029/2008JC004925.

——, and R. Zhang, 2010: Is model parameter error related to a significant spring predictability barrier for El Niño events?—Results from a theoretical model. *Adv. Atmos. Sci.*, **27**(5), 1003–1013.

Hendon, H. H., C. Zhang, and J. D. Glick, 1999: Interannual variation of the Madden-Julian oscillation during austral summer. *J. Climate*, **12**, 2538–2550.

Huang Ronghui, 1999: Advance of the studies of the characteristics, cause of formation and prediction of climate disasters in China. *Chinese Academy of Sciences Bulletin*, **3**, 188–199. (in Chinese)

Kessler, W. S., and R. Kleeman, 2000: Rectification of the MJO into ENSO cycle. *J. Climate*, **13**, 3560–3575.

Latif, M., T. P. Barnett, M. A. Cane, et al., 1994: A review of ENSO prediction studies. *Climate Dyn.*, **9**, 167–179.

Lau, K.-M., and S. Yang, 1996: The Asian monsoon and predictability of the tropical ocean-atmosphere system. *Quart. J. Roy. Meteor. Soc.*, **122**, 945–957.

Luo, J. J., S. Masson, and S. Behera, 2008: Extended ENSO predictions using a fully coupled ocean-atmosphere model. *J. Climate*, **21**, 84–93.

Madden, R. A., 1988: Large intraseasonal fluctuations in wind stress in the tropics. *J. Geophys. Res.*, **93**, 5333–5340.

McPhaden, M. J., 1999: Equatorial waves and the 1997-98 El Niño. *Geophys. Res. Lett.*, **26**, 2961–2964.

Moore, A. M., and R. Kleeman, 1996: The dynamics of error growth and predictability in a coupled model of ENSO. *Quart. J. Roy. Meteor. Soc.*, **122**, 1405–1446.

Mu, M., and W. S. Duan, 2003: A new approach to studying ENSO predictability: Conditional nonlinear optimal perturbation. *Chinese Sci. Bull.*, **48**, 1045–1047.

——, L. Sun, and D. A. Henk, 2004: The sensitivity and stability of the ocean's thermocline circulation to finite amplitude freshwater perturbations. *J. Phys. Oceanogr.*, **34**, 2305–2315.

——, H. Xu, and W. S. Duan, 2007a: A kind of initial perturbations related to "spring predictability barrier" for El Niño events in Zebiak-Cane model. *Geophys. Res. Lett.*, **34**, L03709, doi: 10.1029/2006GL-27412.

——, W. S. Duan, and B. Wang, 2007b: Season-dependent dynamics of nonlinear optimal error growth and El Niño-Southern Oscillation predictability in a theoretical model. *J. Geophys. Res.*, **112**, D10113, doi: 10.1029/2005JD006981.

——, and Z. N. Jiang, 2008: A new approach to the generation of initial perturbations for ensemble prediction: Conditional nonlinear optimal perturbation. *Chinese Sci. Bull.*, **53**(113), 2062–2068.

——, F. Zhou, and H. Wang, 2009: A method to identify the sensitive areas in targeting for tropical cyclone prediction: Conditional nonlinear optimal perturbation. *Mon. Wea. Rev.*, **137**, 1623–1639.

Peng Yuehua, Duan Wansuo, and Xiang Jie, 2011: Effect of stochastic MJO forcing on ENSO predictability. *Adv. Atmos. Sci.*, **28**(6), 1279–1290, doi: 10.1007/s00376-011-0126-4.

Rong, X. Y., R. H. Zhang, T. Li, et al., 2011: Upscale feedback of high-frequency winds to ENSO. *Quart. J. Roy. Meteor. Soc.*, **137**, 894–907, doi: 10.1002/qj.804.

Slingo, J. M., D. P. Rowell, and K. R. Sperber, 1999: On the predictability of the interannual behavior of the Madden-Julian oscillation and its relationship with El Niño. *Quart. J. Roy. Meteor. Soc.*, **125**, 583–610.

Sperber, K. R., J. M. Slingo, and P. M. Inness, 1997: On the maintenance and initiation of the intraseasonal oscillation in the NCEP/NCAR reanalysis and in the GLA and UKMO AMIP simulations. *Climate Dyn.*, **13**(11), 769–795.

Tang, Y., Z. Deng, X. Zhou, et al., 2008: Interdecadal variation of ENSO predictability in multiple models. *J. Climate*, **21**, 4811–4833.

Wang, B., and Z. Fang, 1996: Chaotic oscillation of tropical climate: A dynamic system theory for ENSO. *J. Atmos. Sci.*, **53**, 2786–2802.

Webster, P. J., 1995: The annual cycle and the predictability of the tropical coupled ocean-atmosphere system. *Meteor. Atmos. Phys.*, **56**, 33–55.

——, and S. Yang, 1992: Monsoon and ENSO: Selectively interactive systems. *Quart. J. Roy. Meteor. Soc.*, **118**, 877–926.

Xu Hui, 2006: Studies of predictability problems for Zebiak-Cane ENSO model. Ph. D. dissertation, Institute of Atmospheric Physics, Chinese Academy of Sciences, 145 pp.

Xue, Y., M. A. Cane, and S. E. Zebaik, 1997: Predictability of a coupled model of ENSO using singular vector analysis. Part I: Optimal growth in seasonal background and ENSO cycles. *Mon. Wea. Rev.*, **125**, 2043–2056.

Yu, Y. S., W. S. Duan, H. Xu, et al., 2009: Dynamics of nonlinear error growth and season-dependent predictability of El Niño events in the Zebiak-Cane model. *Quart. J. Roy. Meteor. Soc.*, **135**, doi: 10.1002/qj.526.

Zebiak, S. E., 1989: On the 30–60-day oscillation and the prediction of El Niño. *J. Climate*, **15**, 1381–1387.

——, and M. A. Cane, 1987: A model El Niño-Southern Oscillation. *Mon. Wea. Rev.*, **115**, 2262–2278.

Zhang, C., 2001: Intraseasonal perturbations in sea surface temperatures of the equatorial eastern Pacific and their association with the MJO. *J. Climate*, **14**, 1309–1322.

Zhang Renhe, Zhou Guangqing, and Chao Jiping, 2003: On ENSO dynamics and its prediction. *Chinese J. Atmos. Sci.*, **27**, 674–688. (in Chinese)